

A COARSE-TO-FINE MORPHOLOGICAL APPROACH WITH KNOWLEDGE-BASED RULES AND SELF-ADAPTING CORRECTION FOR LUNG NODULES SEGMENTATION

Xinliang Fu^{*,†}, Jiayin Zheng^{*,†}, Juanyun Mai[†], Yanbo Shao[†], Minghao Wang[†],
Linyu Li[†], Zhaoqi Diao[†], Yulong Chen[§], Jianyu Xiao[§], Jian You[§], Airu Yin^{†,‡},
Yang Yang^ℓ, Xiangcheng Qiu^ℓ, Jinsheng Tao^ℓ, Bo Wang^ℓ, and Hua Ji^{ℓ † ‡}

[†]Advanced Medical Data Research Center, College of Computer Science,
Nankai University, Tianjin, China

[§] Department of {Lung Cancer, Radiology}, Tianjin Lung Cancer Center,
Tianjin Medical University, Tianjin, China

^ℓ AnchorDx Medical Co., Guangzhou, China

Email: {1811112,1811523}@mail.nankai.edu.cn, {yinar, hua.ji}@nankai.edu.cn

ABSTRACT

The segmentation module which precisely outlines the nodules is a crucial step in a computer-aided diagnosis(CAD) system. The most challenging part of such a module is how to achieve high accuracy of the segmentation, especially for the juxta-pleural, non-solid and small nodules. In this research, we present a coarse-to-fine methodology that greatly improves the thresholding method performance with a novel self-adapting correction algorithm and effectively removes noisy pixels with well-defined knowledge-based principles. Compared with recent strong morphological baselines, our algorithm, by combining dataset features, achieves state-of-the-art performance on both the public LIDC-IDRI dataset (DSC 0.699) and our private LC015 dataset (DSC 0.760) which closely approaches the SOTA deep learning-based models' performances. Furthermore, unlike most available morphological methods that can only segment the isolated and well-circumscribed nodules accurately, the precision of our method is totally independent of the nodule type or diameter, proving its applicability and generality.

Index Terms— biomedical image processing, lung nodule segmentation, self-adapting strategy

1. INTRODUCTION

Pulmonary nodules are lung lesions with oval shape. Early diagnosis and investigation of these lung nodules are critical for enhancing patients' chances of survival and allowing effective treatments [1]. However, radiologists must scan hundreds of slices to distinguish between internal non-nodule structures and nodule cells, which takes time and effort. As a result,

there is a high demand for an accurate and efficient computer-aided diagnostic (CAD) system [2]. The lung nodule segmentation module, which automatically outlines the nodule contours, is an important component of a CAD system [3].

Many studies on automatic nodule segmentation have been conducted, and they can be classified into two groups: morphological methods and deep learning-based methods. The morphological methods including thresholding method [4, 5], region growing [6, 7], active contours [8, 9], and graph-cut methods [10, 11], are often based on pixel density; whereas deep learning-based methods [12, 13] use neural networks to extract semantic information [14]. Although morphological techniques do not necessitate as much processing as DNN, their absence of deep semantic traits and 3D information might result in incorrect segmentation, particularly for juxta-pleural [9], ground-glass, and small-sized nodules [15]. To put it another way, their effects are size [5] or type dependent. On the other hand, deep learning models' interpretability and generalizability have been a significant barrier to their widespread adoption in healthcare settings. For instance, its performance is highly dependent on the designs and parameters of neural networks [16]; a model that performs well on one dataset may perform horribly on another one; there is no obvious rationale connecting the data about a case to the model's judgments [17]. Moreover, the interpretability is very critical for doctors to make clinical decisions. Hence, impediments to widely adoption of DL models in real healthcare settings remain strongly due to the black-box nature of DL. To this end, we propose a novel morphological algorithm to address the above issues. Our experimental results have shown that the algorithm can not only produce precise segmentations for nodules of various sorts but also provide excellent interpretability with detailed inference steps illustrations, making it well suited for a real-world CAD system.

^{*}Having equal contribution with the first author [‡] Corresponding author

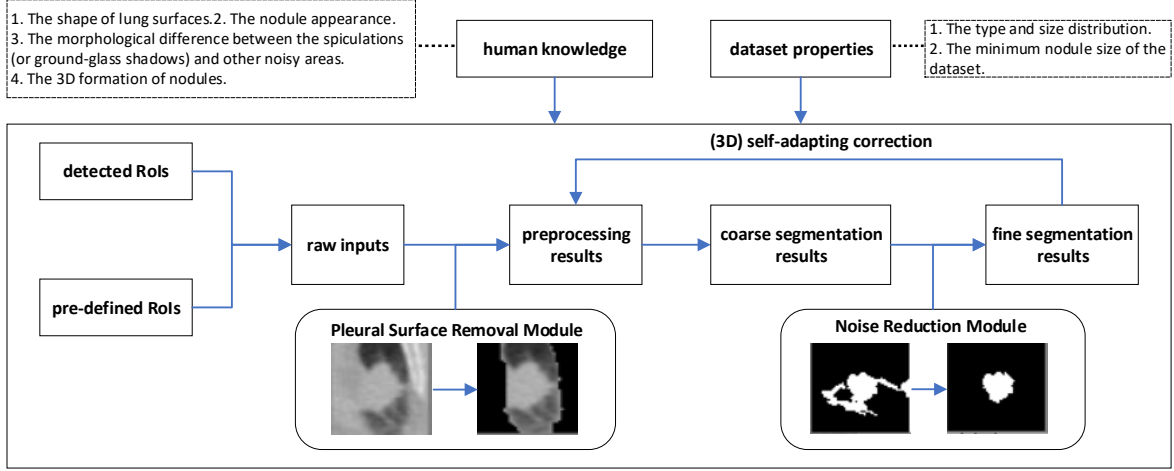


Fig. 1: The overall pipeline of our coarse-to-fine framework. Taking the detection results or the pre-defined RoIs as inputs, our algorithm sequentially conducts lung wall removal, coarse segmentation and fine segmentation.

To summarize, our contributions are as follows:

1. As far as we know, our work is the first attempt to explicitly define knowledge-based principles extracted from clinical experience and knowledge to enhance the morphological method and conduct noise reduction.
2. Our self-adapting thresholding method and its 3D-based version can produce better segmentation especially for small or ground-glass nodules, by referencing adjacent slices and gradually shrinking the bounding box.
3. Our coarse-to-fine morphological method achieves state-of-the-art performance on both the LIDC-IDRI dataset (DSC 0.699) and LC015 dataset (DSC 0.760) and the effects are independent of the nodule type or size.

2. PROPOSED METHOD

We start a coarse-to-fine segmentation method that removes the lung wall, selects candidate pixels, reduces noise, and applies self-adapting correction. As shown in Figure 1, our method does not necessarily need manually selected Region of Interests (RoIs) and can take the detection results as input, making it ideal for an end-to-end intelligent diagnosis system.

2.1. Knowledge-based Principles

Rule 1: An important property of convex figure is that every point on every line segment between two points inside or on the boundary of it remains inside or on the boundary, that is, S is a convex graphic if and only if for all two points p, q belong to S , the connected line \overline{pq} also belongs to S .

Rule 2: If the bounding boxes circumstance the real nodules better, there will be less interference information.

Rule 3: The ground-glass shadow pixels usually evenly surround the solid nodule structures and their mean pixel values

is higher than that of the lung wall but lower than that of the solid nodule structure.

Rule 4: The nodules are oval-shaped and spatially continuous; thus, compared to the original whole RoI box, the bounding box inherited from the more centered slice usually frames the contours of the topper slices more closely.

All the above principles are distilled from human knowledge or experience and will be utilized in the following steps.

2.2. Pleural Surface Removal

Outlining juxtapleural nodules precisely is difficult since the contours may contain the lung walls, reducing the thresholding method's performance. Several people used morphological methods [17] such as the global thresholding method [18] or deep neural networks [19] to segment the lung. However, using the entire CT image as input, these methods need a lot of processing and aren't good enough to eliminate all lung wall cells. Hence, we present a simple yet effective algorithm that needs only the RoI as input and can remove all pleural surface cells in the RoI.

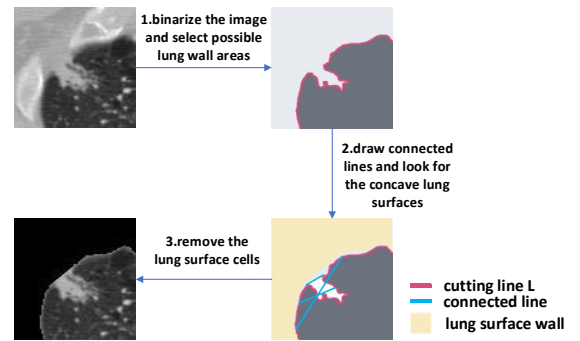


Fig. 2: The grey area includes the concave lung wall area and the raised nodule structure. After drawing connected lines, we find that the yellow area is not covered by any line and remove the pixels in it.

To begin, we binarize the input image, changing the values of pixels above and below the average to 1 (shown grey in Figure 2) and 0 (shown black in Figure 2). L stands for the cutting line that separates the grey and black areas. Since the white raised nodule and the black area together form a convex figure, according to the convex property mentioned in **Rule 1**, the line connecting any two points on L will only still in the white or black area, not crossing the lung surface wall area. Hence, we draw lines between any two spots on L, and the region that is not covered by any line is the lung surface area.

2.3. Coarse Segmentation

There are two methods for coarse segmentation and they differ in how they select candidate pixels. The plain thresholding method treats pixels that are above average as candidate pixels, whereas the deformable method binarizes the image by Otsu’s method first and then does closing, subtraction and opening operations sequentially. Let s_m be the smallest nodule size in this dataset. There may still be multiple isolated areas after pixel selection, and we only keep those that are larger than s_m , referring to them as prospective nodule areas.

2.4. Fine Segmentation

2.4.1. Surrounding Noise Reduction

After selecting the nodule-like areas, we must remove the noisy pixels that surround the nodule structures, including the vasculature. To reduce noise, we need to find dividing lines that separate the nodule area from the noisy areas around it. The dividing line’s start and end points should be on the boundary, and the line should be shorter than α pixels to avoid accidentally excluding part of the nodule. α is a hyper parameter that is set to 8 here. Furthermore, the noisy areas separated by the diving line should be greater than $\pi * (\frac{d+1}{2})^2$, where d is the length of the dividing line, to avoid improper removal of the nodular pixels near the boundary.

2.4.2. Self-adapting Correction

The segmentation of small-sized nodule slices is challenging and the small nodules are divided into two types: 2D slices of nodules with small diameters (usually less than 5mm) and top or bottom slices of larger nodules. We concentrate on the latter in this article since nodules smaller than 5 mm are not the main focus of clinicians. If the bounding boxes circumstance the real nodules better, there will be less interference information (**Rule 2**). As a result, we propose a self-adapting correction method that shrinks the bounding boxes iteratively until they are close enough. Algorithm 1 describes the steps of the self-adapting correction. The iteration will stop if the current bounding box is close enough to frame the nodule contour.

The way to judge whether or not the box is precise enough is by calculating the proportion of the nodule pixels. If the proportion is large enough, we can propose that there are not so many noisy pixels and thus stop the loop.

However, the bounding box cannot be too small for two reasons. Firstly, to be a valid nodule outline, the contour outputted from the bounding box must be larger than s_m where s_m denotes the minimum nodule size. Secondly, for ground-glass nodules, a too-small box may exclude the ground-glass shadow by mistake and thus lead to inaccurate segmentation. The ground-glass shadows usually surround the solid nodule structures evenly (**Rule 3**). Hence, if the pixels of the difference between box_{cur} and box_{next} are equally distributed around the solid nodule structure, we propose that they belong to the ground-glass shadow and stop the iteration.

Algorithm 1 Self-adapting Correction

```

input: Raw input image
output: The contours of a pulmonary nodule
1: function CORRECT(original_box, min_nodule_size,  $\epsilon$ )
2:   cur_box  $\leftarrow$  original_box
3:   cur_contour  $\leftarrow$  THRESHOLD(cur_box)
4:   next_box  $\leftarrow$  FINDBOX(cur_contour)
5:   while Area_next_box < Area_cur_box /  $\epsilon$  do
6:     next_contour  $\leftarrow$  THRESHOLD(next_box)
7:     cur_box  $\leftarrow$  next_box
8:     next_box  $\leftarrow$  FINDBOX(next_contour)
9:     if next_contour < min_nodule_size then
10:      return cur_contour
11:    end if
12:    cur_contour  $\leftarrow$  next_contour
13:  end while
14:  return next_contour
15: end function

```

2.4.3. 3D-based Self-adapting Correction

Inspired by the 3D formation of nodules (**Rule 4**) and how 3D neural network works, we offer a 3D-based self-adapting correction technique that outputs a closer bounding box based on the segments of nearby slices. Figure 3 depicts our method.

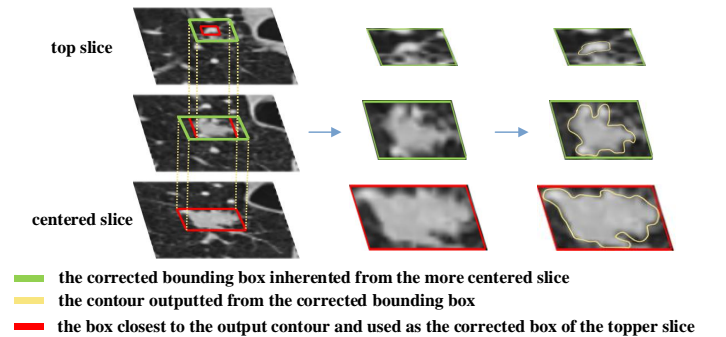


Fig. 3: Example of the 3D-based self-adapting thresholding method. We utilize the segmentation result of the centered slice to help shrink the input bounding box for its adjacent slices and do this process iteratively until the top or bottom slices.

Table 1: Performance comparison between baseline approaches and ours under LIDC-IDRI and LC015 datasets.

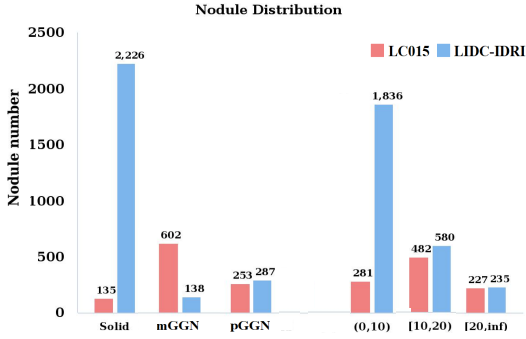
Method	Input	LIDC-IDRI Dataset							LC015 Dataset						
		Avg.	Solid	mGGN	pGGN	(0,10)	[10,20)	[20,inf)mm	Avg.	Solid	mGGN	pGGN	(0,10)	[10,20)	[20,inf)mm
FMM(MM) [20]	pre-defined RoIs	0.396	0.427	0.271	0.179	0.309	0.504	0.468	0.376	0.518	0.399	0.177	0.358	0.369	0.389
PTM(MM)	pre-defined RoIs	0.601	0.604	0.575	0.582	0.527	0.662	0.692	0.720	0.732	0.721	0.704	0.651	0.721	0.736
PDM(MM)	pre-defined RoIs	0.673	0.686	0.627	0.581	0.642	0.702	0.720	0.678	0.719	0.682	0.629	0.631	0.675	0.693
Ours(MM)	pre-defined RoIs	0.699	0.709	0.646	0.640	0.683	0.719	0.712	0.760	0.770	0.760	0.752	0.737	0.760	0.766
Ours(MM)	detected RoIs								0.682	0.701	0.667	0.727	0.704	0.700	0.657
nnUNet(DL) [16]	whole image	0.818	0.826	0.776	0.733	0.799	0.837	0.863	0.781	0.823	0.778	0.762	0.741	0.792	0.798

¹ MM:morphological methods ² DL:deep learning ³ PTM:Plain Thresholding Method ⁴ PDM:Plain Deformable Method ⁵ mGGN:mix ground-glass nodule ⁶ pGGN:pure ground-glass nodule

3. EXPERIMENT

3.1. Dataset

We test the performance of our method on the public LIDC-IDRI dataset [21] and our private LC015 dataset. The LIDC-IDRI dataset provides labeled nodule outlines for 1018 patients (with 2651 nodules), while LC015 dataset is gathered from 14 hospitals and includes 990 patients (with 1186 nodules). In two ways, our private LC015 dataset differs from the present public datasets. First, the nodules are confirmed by clinicians rather than simply labeled by radiologists as such in public datasets by radiologists. Furthermore, the LC015 dataset has a more equally distributed data set than the LIDC-IDRI dataset, in which most nodules are tiny or solid. Therefore, we can see how different techniques function with varied nodule types and sizes by experimenting on two datasets.

**Fig. 4:** Nodule size and type distribution of LIDC-IDRI and LC015 datasets.

3.2. Evaluation Metrics

The Dice Similarity Coefficient (DSC) is a commonly used metric for determining the degree of overlap between the predicted and ground-truth segments. The higher the value is, the more precise the segmentation is [22, 23].

3.3. Performance Comparison

Unlike previous morphological works that do evaluations only on a subset of the dataset [20], we conduct experiments on the whole dataset (3837 nodules in total).

When compared to SOTA morphological approaches, plain thresholding, and deformable methods, our proposed approach produces the best segmentation results on both datasets, as shown in Table 1. When employing pre-defined RoIs, our morphological method closely approaches the nnUNet model on the LC015 dataset. This demonstrates that the morphological method can reach remarkable performance with a faster speed and a clearer rule-based illustration.

Furthermore, earlier morphological approaches typically struggle with juxtapleural, non-solid, and tiny nodules. On the LIDC-IDRI dataset, for example, FFM's performance on non-solid and small nodules drops by 54.9% and 22.0%, respectively. By contrast, our method has consistently high performance that is unaffected by nodule type or diameter. Moreover, even when using the detected RoIs as input where more noisy pixels are introduced, our algorithm can still perform well and output precise segmentations. The results above fully demonstrate the superiority and necessity of incorporating knowledge-based rules and self-adapting correction.

4. CONCLUSIONS

By seamlessly integrating knowledge-based principles and a well designed self-adapting correction algorithm, we present an efficient image processing framework that can yield exact segments for nodules of all sorts and meanwhile provide good explainability of the underlying's inference steps. Compared to other related work, our framework provides two outstanding scientific merits: First, the rule-based and self-correction methods well support accurately segmenting previously intractable nodules including juxtapleural, non-solid, and small nodules. Second, our methods' great precision proves that morphological algorithm can achieve the same accuracy as DL models while using less processing power and meanwhile having much better interpretability and explainability. Therefore, we claim that our approach is well suited for a real-world CAD system that requires precision, automation, and explanation for clinical adoption.

5. REFERENCES

- [1] Maurizio Infante et al., “A randomized study of lung cancer screening with spiral computed tomography: three-year results from the dante trial,” *American journal of respiratory and critical care medicine*, vol. 180, no. 5, pp. 445–453, 2009.
- [2] Stojan Trajanovski et al., “Towards radiologist-level cancer risk assessment in ct lung screening using deep learning,” *Computerized Medical Imaging and Graphics*, vol. 90, pp. 101883, 2021.
- [3] Macedo Firmino et al., “Computer-aided detection system for lung cancer in computed tomography scans: review and future prospects,” *Biomedical engineering online*, vol. 13, no. 1, pp. 1–16, 2014.
- [4] Keelin Murphy et al., “A large-scale evaluation of automatic pulmonary nodule detection in chest ct using local image features and k-nearest-neighbour classification,” *Medical image analysis*, vol. 13, no. 5, pp. 757–770, 2009.
- [5] Anthony P Reeves et al., “On measuring the change in size of pulmonary nodules,” *IEEE transactions on medical imaging*, vol. 25, no. 4, pp. 435–450, 2006.
- [6] Jamshid Dehmeshki et al., “Segmentation of pulmonary nodules in thoracic ct scans: a region growing approach,” *IEEE transactions on medical imaging*, vol. 27, no. 4, pp. 467–480, 2008.
- [7] Bram van Ginneken, “Supervised probabilistic segmentation of pulmonary nodules in ct scans,” in *International Conference on Medical Image Computing and Computer-Assisted Intervention*. Springer, 2006, pp. 912–919.
- [8] M Mehdi Farhangi et al., “3-d active contour segmentation based on sparse linear combination of training shapes (scots),” *IEEE transactions on medical imaging*, vol. 36, no. 11, pp. 2239–2249, 2017.
- [9] Amal A Farag et al., “A novel approach for lung nodules segmentation in chest ct using level sets,” *IEEE Transactions on Image Processing*, vol. 22, no. 12, pp. 5202–5213, 2013.
- [10] Jung won Cha et al., “4d lung tumor segmentation via shape prior and motion cues,” in *2016 38th Annual International Conference of the IEEE Engineering in Medicine and Biology Society (EMBC)*. IEEE, 2016, pp. 1284–1287.
- [11] Xujiong Ye, Gareth Beddoe, and Greg Slabaugh, “Automatic graph cut segmentation of lesions in ct using mean shift superpixels,” *International journal of biomedical imaging*, vol. 2010, 2010.
- [12] Olaf Ronneberger, Philipp Fischer, and Thomas Brox, “U-net: Convolutional networks for biomedical image segmentation,” in *International Conference on Medical image computing and computer-assisted intervention*. Springer, 2015, pp. 234–241.
- [13] Fatemeh Haghighi et al., “Learning semantics-enriched representation via self-discovery, self-classification, and self-restoration,” in *International Conference on Medical Image Computing and Computer-Assisted Intervention*. Springer, 2020, pp. 137–147.
- [14] Fatemeh Haghighi et al., “Transferable visual words: Exploiting the semantics of anatomical patterns for self-supervised learning,” *IEEE transactions on medical imaging*, vol. 40, no. 10, pp. 2857–2868, 2021.
- [15] Li Zheng and Yiran Lei, “A review of image segmentation methods for lung nodule detection based on computed tomography images,” in *MATEC Web of Conferences*. EDP Sciences, 2018, vol. 232, p. 02001.
- [16] Fabian Isensee et al., “nnu-net: Self-adapting framework for u-net-based medical image segmentation,” *arXiv preprint arXiv:1809.10486*, 2018.
- [17] Di Jin et al., “Explainable deep learning in healthcare: A methodological survey from an attribution view,” *WIREs Mechanisms of Disease*, p. e1548, 2022.
- [18] Giorgio De Nunzio et al., “Automatic lung segmentation in ct images with accurate handling of the hilar region,” *Journal of digital imaging*, vol. 24, no. 1, pp. 11–27, 2011.
- [19] Samuel G Armato et al., “Computerized detection of pulmonary nodules on ct scans,” *Radiographics*, vol. 19, no. 5, pp. 1303–1311, 1999.
- [20] Skourt et al., “Lung ct image segmentation using deep neural networks,” *Procedia Computer Science*, vol. 127, pp. 109–113, 2018.
- [21] Samuel G. Armato III, Geoffrey McLennan, et al., “The lung image database consortium (lidc) and image database resource initiative (idri): A completed reference database of lung nodules on ct scans,” *Medical Physics*, vol. 38, no. 2, pp. 915–931, 2011.
- [22] Savic et al., “Lung nodule segmentation with a region-based fast marching method,” *Sensors*, vol. 21, no. 5, pp. 1908, 2021.
- [23] Shuo Wang et al., “Central focused convolutional neural networks: Developing a data-driven model for lung nodule segmentation,” *Medical image analysis*, vol. 40, pp. 172–183, 2017.